AGU PUBLICATIONS

JGR

Journal of Geophysical Research: Space Physics

RESEARCH ARTICLE

10.1002/2014JA019903

Key Points:
- Observational evidence of e-Landau resonant interactions with chorus waves
- Identifying Landau resonant velocity from the electron phase space density
- Statistical analysis of signatures of the Landau resonant interactions

Correspondence to:
K. Min,
kmin@auburn.edu

Citation:
Min, K., K. Liu, and W. Li (2014), Signatures of electron Landau resonant interactions with chorus waves from THEMIS observations, *J. Geophys. Res. Space Physics*, *119*, 5551–5560, doi:10.1002/2014JA019903.

Received 19 FEB 2014
Accepted 27 JUN 2014
Accepted article online 30 JUN 2014
Published online 18 JUL 2014

Signatures of electron Landau resonant interactions with chorus waves from THEMIS observations

Kyungguk Min[1], Kaijun Liu[1], and Wen Li[2]

[1]Department of Physics, Auburn University, Auburn, Alabama, USA, [2]Department of Atmospheric and Oceanic Sciences, University of California, Los Angeles, California, USA

Abstract Simultaneous observations of electron phase space density (PSD) and chorus waves for more than 4 years by the Time History of Events and Macroscale Interactions during Substorms (THEMIS) are analyzed to identify signatures of the electron Landau resonant interactions with chorus waves in the radiation belts. Chorus waves play an important role in the radiation belt dynamics by effectively interacting with electrons. Landau resonant interactions arise when the waves are not exactly parallel propagating. Such interactions lead to "plateaus" along $v_{\parallel}$ in the electron velocity distributions, where $v_{\parallel}$ is the parallel (with respect to the background magnetic field) component of the electron velocity. The analyzed electron PSDs often demonstrate local minima in the derivative of the velocity distribution along $v_{\parallel}$ near the Landau resonant velocity calculated from the simultaneous in situ wave observations. These minima are, therefore, direct signatures and solid evidence of the electron Landau resonant interactions with chorus waves.

1. Introduction

Whistler mode chorus waves are naturally occurring intense electromagnetic waves below the electron cyclotron frequency which can be excited through an instability driven by an anisotropic distribution of electrons [e.g., *Kennel and Petschek*, 1966]. In the terrestrial magnetosphere outside the plasmasphere, these waves are observed typically in the frequency range of 0.1 f_{ce}–0.8 f_{ce} [*Tsurutani and Smith*, 1977; *Koons and Roeder*, 1990] and often show banded spectra with a gap near 0.5 f_{ce} [*Tsurutani and Smith*, 1974; *Koons and Roeder*, 1990], where f_{ce} is the equatorial electron cyclotron frequency. They are usually composed of discrete wave elements with rising or falling tones (chorus) accompanied by incoherent banded whistler waves in the background [e.g., *Santolík et al.*, 2003].

Chorus waves are believed to be generated near the magnetic equator [*LeDocq et al.*, 1998; *Lauben et al.*, 2002; *Santolík et al.*, 2003]. Observational studies show that the upper band (above 0.5 f_{ce}) and lower band (below 0.5 f_{ce}) waves have different characteristics. The upper band waves have a broad wave normal distribution from field aligned to oblique angles while the lower band waves are either quasi field aligned or very oblique, close to the resonance cone [*Li et al.*, 2013]. The lower band waves are typically stronger than the upper band waves [e.g., *Li et al.*, 2011; *Meredith et al.*, 2012; *Agapitov et al.*, 2013]. Recent studies suggest that the chorus elements arise from the incoherent background waves through nonlinear wave growth involving the inhomogeneity of the background magnetic field [*Omura et al.*, 2008]. On the other hand, several scenarios have been proposed to explain the banded spectra with a gap near 0.5 f_{ce} [*Liu et al.*, 2011, and references therein]. Chorus waves play a significant role in the pitch angle scattering and acceleration of radiation belt electrons through resonant interactions with electrons [*Horne and Thorne*, 1998; *Horne et al.*, 2005].

One fundamental form of wave-particle resonant interactions occurs through Landau resonance which arises when particles move at the same speed as the wave along the background magnetic field direction and when the wave has a nonzero parallel electric field component. Landau resonant interactions reduce $\left|\partial f/\partial v_{\parallel}\right|$ around the resonant velocity and often lead to the formation of "plateaus" in the particle velocity distribution [*Kennel and Engelmann*, 1966; *Swanson*, 2003], where f is the particle velocity distribution and $v_{\parallel}$ is the parallel component of the particle velocity with respect to the background magnetic field. As described below, the present study investigates the plateaus formed in this quasi-linear manner from the Landau resonant interactions between electrons and chorus waves in the radiation belts. On the other hand, it is worth mentioning that for high-amplitude oblique whistlers [*Cattell et al.*, 2008], the parallel electric field component of the waves can trap electrons in Landau resonance and lead to significant nonlinear

acceleration of these electrons [*Artemyev et al.*, 2012, 2013; *Agapitov et al.*, 2014]. In addition, Landau resonance plays a very important role in controlling chorus wave growth and propagation [e.g., *Bortnik et al.*, 2006].

Generally, chorus waves observed in the radiation belts are not exactly parallel propagating [e.g., *Santolík et al.*, 2009; *Li et al.*, 2011]. Therefore, they have nonzero parallel electric field component [*Verkhoglyadova et al.*, 2010] with which electrons are subject to Landau resonant interactions. In the present work, we seek the signatures of such interactions by examining simultaneous observations of electron phase space density (PSD) and chorus waves for more than 4 years by the Time History of Events and Macroscale Interactions during Substorms (THEMIS). The electron PSDs analyzed often demonstrate local minima in $\left|\partial f/\partial v_{\parallel}\right|/f$ along $v_{\parallel}$ near the Landau resonant velocity calculated from the simultaneous in situ wave observations. These minima are, therefore, direct signatures and solid evidence of the electron Landau resonant interactions with chorus waves. The paper is organized as follows. Section 2 describes instrumentation, event selection, and estimation of the Landau resonant velocity. Section 3 presents the statistical result, and section 4 concludes the paper.

2. Data Processing and Event Selection

2.1. Instrumentation

The THEMIS spacecraft consist of five identical probes in near-equatorial orbits with apogee above 10 R_E and are equipped with sophisticated particle and field instruments [*Angelopoulos*, 2008]. The present paper particularly utilizes waveforms from the Search-Coil Magnetometer (SCM) [*Roux et al.*, 2008; *Le Contel et al.*, 2008] that provides three orthogonal components of magnetic field fluctuations with the maximum frequency of 4 kHz, large enough to observe the whistler waves above $\sim 5R_E$, and electron distributions from the electrostatic analyzer (ESA) [*McFadden et al.*, 2008] that measures full 3-D distributions of electrons from a few eV up to 30 keV. The background magnetic fields are provided by the fluxgate magnetometer (FGM) [*Auster et al.*, 2008] which measures direct current (dc) and low-frequency fluctuations up to 64 Hz. Electron densities are provided from the database constructed by *Li et al.* [2010], which are estimated from the spacecraft potential measured by the Electric Field Instruments [*Bonnell et al.*, 2008] and electron thermal speed measured by the ESA, and have an uncertainty of a factor of 2.

2.2. Preprocessing

Individual burst-mode wave data, usually consisting of either ~7 s or ~15 s continuous measurements, were Fourier transformed to get power spectra, polarization, and wave normal angle using the technique described by *Santolík et al.* [2001] and *Santolík and Gurnett* [2003]. The background magnetic field measured by the FGM instrument was used to calculate the transformation matrix into the field-aligned coordinate system. The local and equatorial electron cyclotron frequencies were calculated using the measured background magnetic field and the field from the Tsyganenko 05 model [*Tsyganenko and Sitnov*, 2005] with the model parameters from *Qin et al.* [2007]. Taking into account the fact that we know the value of the magnetic field at the spacecraft location $B_{\mathrm{obs,sc}}$, we adjust the magnetic field values from the Tsyganenko model by multiplying by $B_{\mathrm{obs,sc}}/B_{\mathrm{mod,sc}}$. In this way, we only use the shape of the field line from the model and the magnitude is determined from observation [*Denton et al.*, 2001].

Since the duration of the burst mode is approximately two to four spins long, it is natural to define an event as each burst-mode observation. For each event, the total wave power was integrated along the time dimension, resulting in $IP(f)$, from which peaks and bandwidths (distance between two frequencies at $IP_{\mathrm{pk}} \cdot e^{-1}$) were found. The wave normal angle weighted with wave power was also averaged along the time dimension. Finally, the noise floor for each event was estimated by fitting a straight line to the $\log f - \log IP$ distribution excluding ranges of the enhanced power. After the noise floor has been obtained, the observed spectral peaks were justified by applying criteria described in section 2.5 to the spectral peaks and bandwidths. As an example, Figures 1a–1c show the total wave power spectra, ellipticity, and wave normal angle as functions of frequency and time, and Figures 1d and 1e show the time-integrated and residual wave powers (the residual power is defined as the ratio of *IP* to the noise floor). The estimated noise floor (gray dashed curve in Figure 1d) represents the background noise level fairly well. Consequently, the residual power clearly signifies the lower band waves. The horizontal gray bar in Figure 1e represents the estimated bandwidth. Displayed as a red curve in Figure 1d, the averaged wave normal angle within the lower band was around 20° with a standard deviation less than 5°.

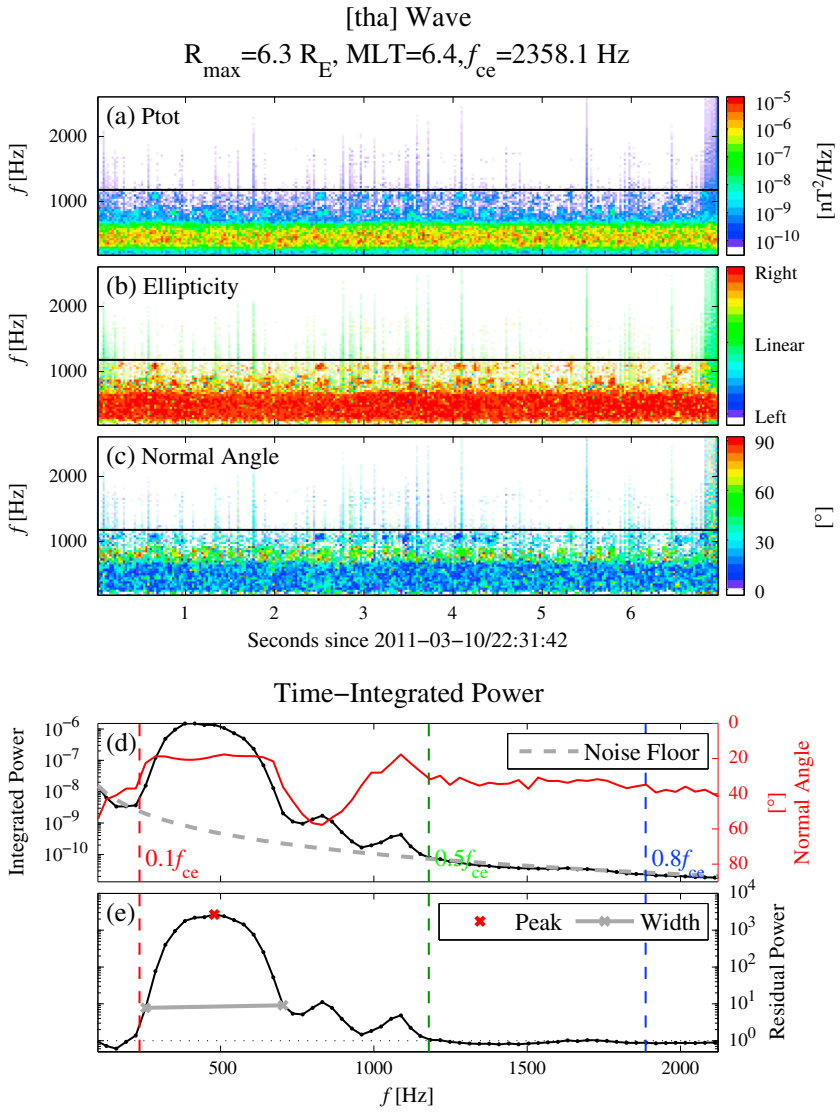

Figure 1. An example chorus wave event observed by Spacecraft A on 10 March 2011. (a–c) The total wave power, ellipticity, and wave normal angle. The solid lines above 1 kHz indicate 0.5 f_{ce} where f_{ce} is the equatorial electron cyclotron frequency. The white region indicates that the wave power is less than 10^{-10} nT^2/Hz. (d) The black and red curves represent the integrated power and power-weighted average of wave normal angle as a function of frequency, respectively. The dashed gray curve represents the noise floor. (e) The residual power as a function of frequency. The red cross symbol and horizontal gray bar indicate the peak and bandwidth of the waves. The three colored vertical lines in Figures 1d and 1e, from left to right, mark 0.1 f_{ce}, 0.5 f_{ce}, and 0.8 f_{ce}, respectively.

Once tabulated, the wave event list was used to collect the electron fluxes during the same time period from the burst-mode ESA observations which are provided with one spin resolution (~3 s). The two or three spin long differential fluxes for each event were then averaged in time and converted into PSDs, $f(v_{\parallel}, v_{\perp})$. Finally, in order to identify signatures of electron Landau resonant interactions with the waves, the absolute values of the derivatives of the PSDs with respect to $v_{\parallel}$ were calculated and normalized to the PSDs ($\left|\partial f/\partial v_{\parallel}\right|/f$). As an example, Figures 2a and 2b display $f(v_{\parallel}, v_{\perp})$ and $\left|\partial f(v_{\parallel}, v_{\perp})/\partial v_{\parallel}\right|/f$ during the wave event shown in Figure 1. The same quantities are also displayed in the energy pitch angle space in Figures 2d and 2e. Clearly noticeable are two minima in $\left|\partial f/\partial v_{\parallel}\right|/f$ around the dashed lines which indicate the Landau resonant velocity calculated using the simultaneous in situ wave observations (as described in section 2.3). These minima extend across the whole range of $v_{\perp}$ examined but are more pronounced at small $v_{\perp}$ (below the white dashed line). The close match of the locations of these minima with the Landau resonant

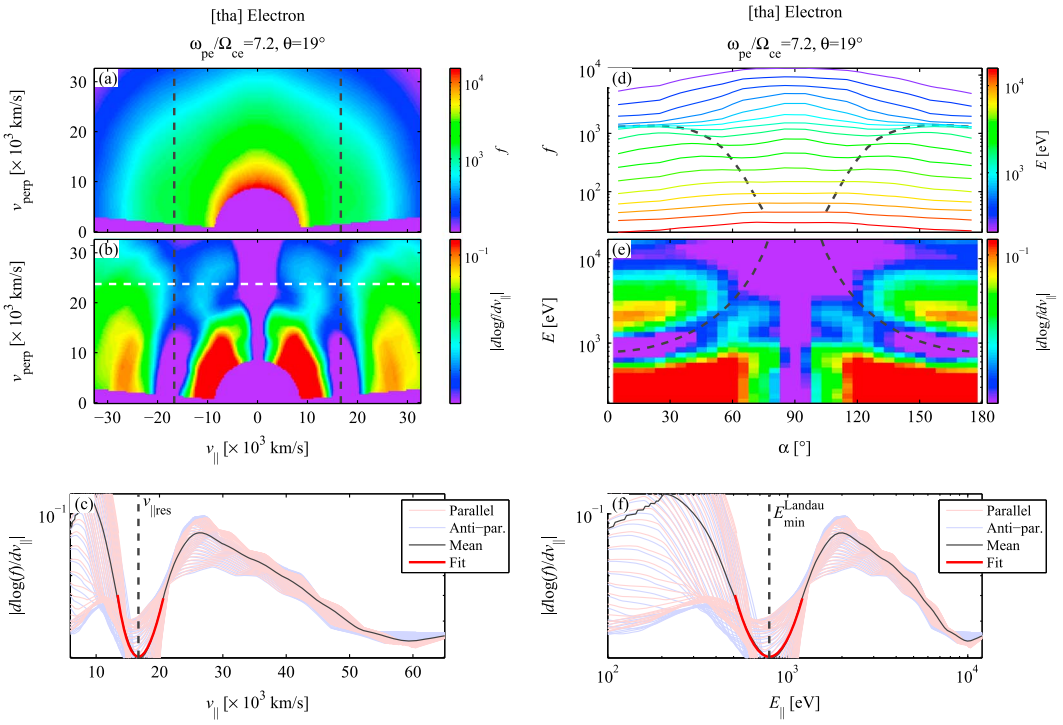

Figure 2. The measured electron phase space density during the wave event shown in Figure 1. (a–b) The electron PSD and its derivative with respect to $v_{\parallel}$ (i.e., $\left|\partial f/\partial v_{\parallel}\right|/f$) as a function of velocity. (c) Line profiles of $\left|\partial f/\partial v_{\parallel}\right|/f$ at different $v_{\perp}$. The parallel (light red curves) and antiparallel (light blue curves) components are superimposed on top of each other, and the average of all the curves with $v_{\perp} < 23 \times 10^3$ km/s is represented by the black solid curve. (d–f) The same quantities as those on the left but displayed in the energy and pitch angle space instead. The vertical dashed curves in all panels represent the calculated $\langle v_{\parallel \mathrm{res}} \rangle$ or the corresponding minimum Landau resonant energy as described in section 2.3. The horizontal dashed line in Figure 2b marks at 23×10^3 km/s which corresponds to an electron energy of 1.6 keV. Units of f and $\left|\partial f/\partial v_{\parallel}\right|/f$ are $(\mathrm{c/MeV\,cm})^3$ and $\mathrm{eV}^{-1/2}$, respectively.

velocities indicates that these minima are the direct consequences of electron Landau resonant interactions with the waves.

The electron PSD displayed in Figure 2a and the absolute value of its derivative along $v_{\parallel}$ shown by Figure 2b are very symmetric about $v_{\parallel} = 0$ (the minimum at $v_{\parallel} = 0$ in Figure 2b is due to this symmetry). This is indeed true for all the events examined. Typically, both parallel and antiparallel propagating waves are expected within the source region [*LeDocq et al.*, 1998; *Parrot et al.*, 2003; *Santolík et al.*, 2005; *Agapitov et al.*, 2013]. These waves Landau resonate with both parallel and antiparallel moving electrons with respect to the background magnetic field at the Landau resonant velocity. The resultant electron distribution should then be generally symmetric. However, most of our events did not occur in the source region, as the Poynting fluxes for our events are mostly unidirectional (not shown). The observed symmetry of the electron PSDs about $v_{\parallel} = 0$ is likely due to the electron bounce motion in the radiation belts. Although the waves excited in the source region propagate toward each hemisphere and become unidirectional, the electrons bounce between the mirror points in the two hemispheres so they are still subject to Landau resonant interactions with waves propagating in both directions. Therefore, if the typical electron bouncing period is shorter than the wave event duration, the resultant electron distribution is still expected to be approximately symmetric. In the present study, the observed wave parameters and electron PSDs have been integrated and averaged over the duration of the burst mode which is typically ~7 s long, as the main goal is to identify quasi-linear signatures of electron Landau resonant interactions with chorus waves.

2.3. Calculating the Landau Resonant Velocity From Wave Observation

Landau resonance occurs when particles move at the same speed as the wave along the background magnetic field direction. Landau resonant velocity is essentially the parallel wave phase velocity, $u_{\parallel} = \omega/k_{\parallel}$,

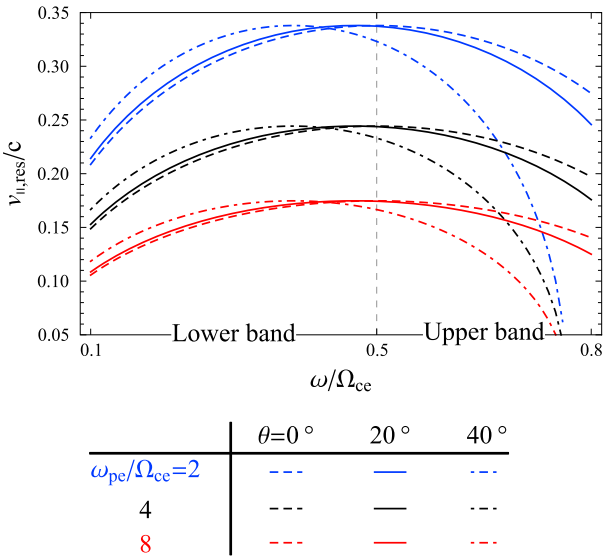

Figure 3. Dependence of $v_{\|res}$ on $(\omega_{pe}/\Omega_{ce})^2$ (or electron density if the background magnetic field is fixed) and wave normal angle. Dashed, solid, and dashed-dotted curves, respectively, represent three wave normal angles: $\theta = 0,\ 20,\ 40°$. Blue, black, and red colors, respectively, represent three $(\omega_{pe}/\Omega_{ce})^2$ ratios: $(\omega_{pe}/\Omega_{ce})^2 = 2,\ 4,\ 8$.

where ω is the wave frequency and $k_\|$ is the parallel wave number. Given the wave normal angle θ, which is the angle between the wave number vector **k** and the background magnetic field, $k_\| = k\cos\theta$. While ω and θ can be directly determined from wave observations, k needs to be estimated using the wave dispersion relation. Here the approximate cold plasma dispersion relation for quasi-parallel propagating whistler waves has been assumed for simplicity [*Stix*, 1962],

$$\frac{c^2}{u^2} = \frac{\omega_{pe}^2}{\Omega_{ce}^2}\frac{\Omega_{ce}}{\omega}\frac{1}{(\cos\theta - \omega/\Omega_{ce})}, \quad (1)$$

where c is the speed of light, u is the wave phase speed, ω_{pe} is the electron plasma frequency, and Ω_{ce} is the electron cyclotron frequency. Equation (1) becomes less accurate for large wave normal angle, but the present work considers waves with $\theta < 45°$ only. From equation (1), the Landau resonant velocity is then

$$v_{\|res} = c\sec\theta\sqrt{\frac{\Omega_{ce}^2}{\omega_{pe}^2}\frac{\omega}{\Omega_{ce}}\left(\cos\theta - \frac{\omega}{\Omega_{ce}}\right)}. \quad (2)$$

Since electron PSDs are often analyzed in terms of electron energy instead of electron velocity, we convert the Landau resonant velocity in equation (2) to the corresponding electron energy

$$E_{min}^{Landau} = \frac{m_e c^2}{2}\frac{\Omega_{ce}^2}{\omega_{pe}^2}\frac{\omega}{\Omega_{ce}}\sec^2\theta\left(\cos\theta - \frac{\omega}{\Omega_{ce}}\right), \quad (3)$$

where m_e is the electron rest mass [*Li et al.*, 2010]. This energy is often referred to as the minimum Landau resonance energy as this is the minimum energy that an electron needs to be in Landau resonance with the wave. Here ω_{pe}/Ω_{ce} is determined using the measured total electron density and the background magnetic field as described in sections 2.1 and 2.2, respectively.

Figure 3 displays how $v_{\|res}$ varies with ω for selected values of $\omega_{pe}/\Omega_{ce} = \{2,4,8\}$ and $\theta = \{0,20,40\}°$. First of all, $v_{\|res}$ is inversely proportional to ω_{pe}/Ω_{ce}. In addition, $v_{\|res}$ monotonically increases with ω, peaks at $\cos\theta/2$ (i.e., at Gendrin angle) and decreases with ω afterward. For the range of wave normal angles displayed, $v_{\|,res}$ is not sensitive to θ in the lower band frequency range but becomes sensitive in the upper band frequency range. Thus, for lower band waves, the uncertainty in the θ measurement is not expected to affect the calculated $v_{\|,res}$ much, whereas it can lead to a significant error for upper band waves. Nevertheless, the present study includes both upper band and lower band chorus waves, because the number of upper band wave events found is very small, which is consistent with previous statistical studies [e.g., *Meredith et al.*, 2012].

The observed waves often have finite bandwidths and are not monochromatic. To account for this, we first compute E_{min}^{Landau} for waves at different frequencies using equation (3), then calculate the wave power-weighted average of E_{min}^{Landau}. Although the contribution would be minuscule, the region outside of the wave band (i.e., outside of the gray bar in Figure 1e) was excluded in the average. Finally, $\langle v_{\|res}\rangle = \sqrt{2\langle E_{min}^{Landau}\rangle/m_e}$ is used as the Landau resonant velocity calculated from the wave observations in the rest of the paper, where $\langle E_{min}^{Landau}\rangle$ is the wave power-weighted average of E_{min}^{Landau} calculated. It is as expected that

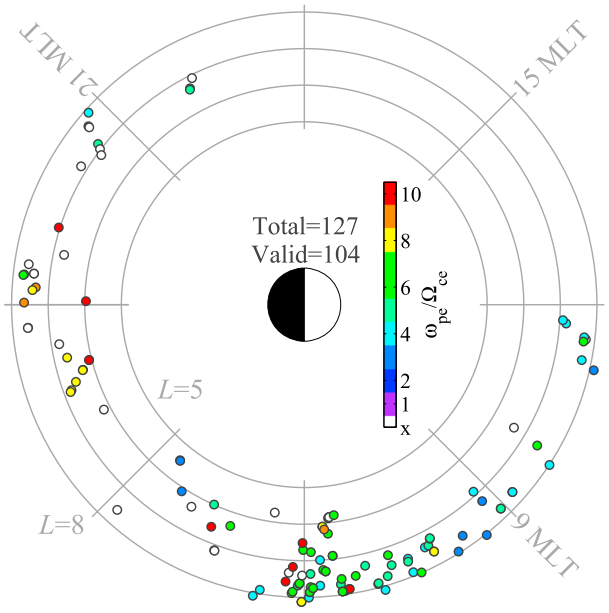

Figure 4. Distribution of identified events on the L-MLT plane. Filled circles, 129 out of 152 events, are the events that have identifiable Landau resonance signatures. The fill color represents the ratio of measured ω_{pe} to Ω_{ce}.

this value is typically close to the Landau resonant velocity associated with the strongest wave at the spectral peak. For the wave event shown in Figure 1, the Landau resonant velocity calculated is 16.7×10^3 km/s, equivalent to an electron energy of 789 eV. Corresponding to the symmetric electron PSD observed, the two vertical dashed lines in Figures 2a and 2b mark the locations of both $\langle v_{\parallel res} \rangle$ and $-\langle v_{\parallel res} \rangle$.

2.4. Determining the Locations of $\left|\partial f/\partial v_{\parallel}\right|/f$ Minima From Electron PSDs

In Figure 2b, the match of the locations of the two $\left|\partial f/\partial v_{\parallel}\right|/f$ minima at $v_{\parallel} \approx \pm 17 \times 10^3$ km/s (corresponding to an electron energy of $E_{\parallel} = 790$ eV) with the Landau resonant velocity calculated from the wave observations and marked by the vertical dashed lines indicates that the minima are the consequence of electron Landau resonant interactions with the chorus waves simultaneously observed. To facilitate such a comparison for more events, we developed a method to numerically determine the locations of $\left|\partial f/\partial v_{\parallel}\right|/f$ minima as shown in Figure 2c.

The observed electron distributions are generally symmetric about $v_{\parallel} = 0$. Corresponding to this feature, Figure 2c shows the profiles of $\left|\partial f/\partial v_{\parallel}\right|/f$ as a function of $\left|v_{\parallel}\right|$ at different $v_{\perp}$. The light blue (red) curves are the $v_{\parallel} > 0$ (< 0) portion of $\left|\partial f/\partial v_{\parallel}\right|/f$. Since the minima are clearer at smaller $v_{\perp}$, we only consider the profiles of $v_{\perp} < 23 \times 10^3$ km/s and calculate their average. This cutoff in $v_{\perp}$ is roughly determined by examining all the selected events. The horizontal white dashed line in Figure 2b represents $v_{\perp} = 23 \times 10^3$ km/s (corresponding to an electron energy of $E_{\perp} = 1.6$ keV). The black solid curve represents the final average profile. The "dip" centered around the local minimum is modeled with the red concave curve using a Gaussian function from which the location and width of the dip are finally estimated. The finite width of the dip is likely related to the bandwidth of the observed waves because waves at different frequencies resonate with electrons at different $v_{\parallel}$. For the example shown in Figure 2b, the local minimum is estimated at $v_{\parallel}$=17×10^3 km/s (corresponding to an electron energy of $E_{\parallel} = 790$ eV) which is very close to the Landau resonant velocity calculated from the wave observations ($\langle v_{\parallel res} \rangle = 16.7 \times 10^3$ km/s). Since the number of events is small, we manually inspected the similar patterns of the local minima in $\left|\partial f/\partial v_{\parallel}\right|/f$ as shown in Figure 2c and then applied the fitting procedure to all the selected events.

2.5. Event Selection

Observations between 1 June 2008 and 31 December 2012 by three spacecraft, A, D, and E, were processed. To make sure that the waves were observed in the plasma trough and near the magnetic equator, the radial distance and the magnetic latitude (MLAT) are limited to $5\ R_E \le |\mathbf{R}_{sc}| \le 8\ R_E$ and $|\mathrm{MLAT}| \le 10°$, respectively, where $\mathbf{R}_{sc}$ is the spacecraft position vector and R_E is the Earth radius. Since the magnetopause can easily cross $L = 8$ during disturbed solar wind conditions, we ensured that the standard deviations of the high (125 samples/s) and low (four samples/s) resolution FGM data for each event are less than 1 nT. Note that we have used the same criteria as *Li et al.* [2010] did to make sure that the observations were indeed made outside the plasmasphere in order to exclude plasmaspheric hiss emissions. We selected whistler mode waves, including rising and falling tones and hiss-like emissions [*Li et al.*, 2012] without differentiating them, as long as they were observed in the plasmatrough region. We only selected the events where the observed

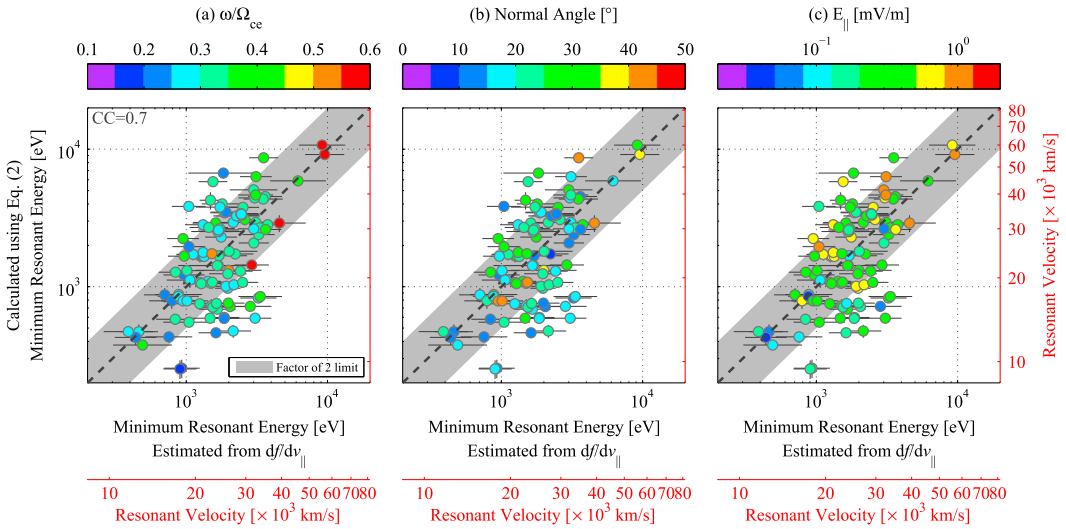

Figure 5. The comparison of the locations of the $\left|\partial f/\partial v_{\|}\right|/f$ minima estimated from the electron PSDs with the Landau resonant velocities calculated from the simultaneous wave observations. The comparison is displayed in terms of both electron velocity and the corresponding energy. All panels are identical except that (a–c) the fill colors represent the ω/Ω_{ce} ratio, wave normal angle, and the parallel electric field amplitude, respectively. Horizontal and vertical lines stretched out from each circle represent the error bars of the estimated locations of the $\left|\partial f/\partial v_{\|}\right|/f$ minima and the minimum Landau resonant energy calculated from the wave measurements, respectively. The diagonal dashed lines represent a one-to-one relation, and the gray diagonal boxes represent a factor-of-two limit related to the factor-of-two uncertainty in the electron densities estimated from the spacecraft potential. The circles are grouped along the diagonal dashed line with a correlation coefficient of 0.7.

wave normal angle is below 45°. The following criteria are imposed to further filter out any inappropriate events for this study: (1) 0.1 f_{ce} > 100 Hz and 0.8 f_{ce} < 2 kHz (Nyquist frequency), (2) ω_{pe}/Ω_{ce} > 1, (3) only single-banded waves (lower band residual power >10 and upper band residual power >5), (4) and bandwidth < 0.3 f_{ce}.

The second condition ensures that $v_{\|res}$ is within the range that the instrument can measure (note that $v_{\|res}$ is inversely proportional to ω_{pe}/Ω_{ce}, and the upper energy limit of ESA is ~30 keV). Since broadband waves can lead to resonant diffusion in a wide energy range and blur the sharp feature of the local minimum in $\left|\partial f/\partial v_{\|}\right|/f$ (Figure 2c), the last two conditions keep the interaction region small in $v_{\|}$ space and can help identify the $\left|\partial f/\partial v_{\|}\right|/f$ minima.

Figure 4 shows all identified events distributed in the L-MLT (magnetic local time) plane. Out of 127 events satisfying the above criteria, 104 events shown as filled circles have identifiable Landau resonance signatures in $\left|\partial f/\partial v_{\|}\right|/f$. Measured ω_{pe}/Ω_{ce} ratios indicated by the fill color are mostly within a range of 2–8. More events have been selected in the morning sector, which is consistent with the chorus occurrence probability observed [*Li et al.*, 2009; *Meredith et al.*, 2012].

3. Results

Figure 5 displays the final result of the analysis. For the selected events, the locations of the $\left|\partial f/\partial v_{\|}\right|/f$ minima estimated from the electron PSDs are compared against the Landau resonant velocities calculated from the simultaneous wave observations as described in section 2.3. The comparison has been displayed in terms of both electron velocity and the corresponding energy. All scatterplots are identical except that the fill colors, from left to right, represent dependence on the normalized frequency (ω/Ω_{ce}), wave normal angle, and amplitude of the parallel electric field component (derived using equation (13) in *Verkhoglyadova et al.* [2010]), respectively. The horizontal error bars stretched out from the center of each circle represent 1 standard deviation of the Gaussian model of the dip discussed in section 2.4 and are estimated

to be less than a factor of 2 for most cases. The vertical error bars represent 1 standard deviation of the power-weighted average of E_{min}^{Landau} discussed in section 2.3 and are mostly less than the size of the circles.

First of all, the circles in Figure 5 are grouped along the diagonal dashed line with a correlation coefficient of 0.7. So the locations of the $\left|\partial f/\partial v_{\|}\right|/f$ minima estimated from the electron PSDs generally match the Landau resonant velocities calculated from the simultaneous wave observations. This indicates that these minima are the direct signatures and solid evidence of the electron Landau resonant interactions with the chorus waves.

On the other hand, the statistical deviation of the circles from the dashed line is quite significant in Figure 5. This deviation is partially related to the factor-of-two uncertainty in the electron densities estimated from the spacecraft potential [*Li et al.*, 2010]. As shown by equation (3), the minimum Landau resonance energy is inversely proportional to $\omega_{pe}^2/\Omega_{ce}^2$ and, subsequently, inversely proportional to the electron density if the background magnetic field is fixed. Therefore, the factor-of-two uncertainty in the electron densities led to a same uncertainty in the minimum Landau resonance energy calculated, which is represented by the gray box in Figure 5. However, a substantial portion of the circles are beyond this factor-of-two limit, suggesting that some other factors also contribute to the deviation.

From Figure 5a, there is clearly a tendency that larger (smaller) frequencies (ω/Ω_{ce}) of waves are related to larger (smaller) $v_{\|res}$ values, i.e., yellow green circles are near the top right corner while bluish circles are near the bottom left corner. This can be directly explained by equation (2) and Figure 3. Note that the majority of the events selected have chorus waves in the lower band. For waves below ~0.5 f_{ce}, the Landau resonant velocity monotonically increases with the wave frequency. On the other hand, there is no clear dependence of the results on the wave normal angle and $|E_{\|}|$, as suggested by Figures 5b and 5c. The latter is a little surprising because Landau resonant interactions are more effective when $|E_{\|}|$ is large, so one expects the data circles associated with larger $|E_{\|}|$ to be closer to the diagonal dashed line in Figure 5c.

4. Conclusions and Discussions

Simultaneous observations of electron PSD and chorus waves have been examined for signatures of electron Landau resonant interactions with whistler mode chorus waves. For most of the events, there exists a range of parallel velocity ($v_{\|}$) within which the PSDs form plateaus and the derivatives of the PSDs with respect to $v_{\|}$ form local minima. Our statistical study shows that the locations of such minima generally match the Landau resonant velocities (or the minimum Landau resonant energies) calculated from the in situ wave measurements. Therefore, the plateaus identified in the electron PSDs are mostly the consequences of electron Landau resonant interactions with the chorus waves. These plateaus provide solid evidence of the scattering of electrons by chorus waves through Landau resonance in the radiation belts.

Despite the general match between the locations of the $\left|\partial f/\partial v_{\|}\right|/f$ minima estimated from the electron PSDs with the Landau resonant velocities calculated from the simultaneous wave observations, there are a substantial amount of events for which these two quantities differ significantly. The significant deviation is partially related to the factor-of-two uncertainty in the electron densities estimated from the spacecraft potential [*Li et al.*, 2010] as discussed in section 3, but other factors may also contribute.

The resonant condition can vary significantly along the magnetic latitude since the wave normal angle distribution depends on magnetic latitude [*Artemyev et al.*, 2012; *Agapitov et al.*, 2014], and the observations show that the waves have larger wave normal angle at higher latitude [*Li et al.*, 2011; *Agapitov et al.*, 2013]. It is possible that electrons may have Landau resonated with waves at high latitudes and are then bounced back to the spacecraft locations near the equator. However, as indicated in *Artemyev et al.* [2012, Figure 2 (middle)], the Landau resonant velocity monotonically increases with latitude. If Landau resonance has occurred at high latitudes and the electrons are then bounced back, the locations of $|\partial f/\partial v_{\|}|$ minima should be always larger than the locally calculated ones using observed wave parameters. Figure 5 does not show a systematic shift of the data circles with respect to the diagonal dashed lines. Thus, this scenario is unlikely what causes the significant deviation.

Another possible explanation is that the electrons in the radiation belts interact with chorus waves whose properties vary with time. The electron PSDs observed therefore carry memories from the previous interactions with the waves that the electrons have encountered earlier. The locations of the $\left|\partial f/\partial v_{\|}\right|/f$

minima can then be different from the Landau resonant velocities calculated from the simultaneous wave parameters.

Finally, it is worth mentioning that besides Landau resonance, electrons interact with chorus waves through other resonances as well, e.g., the first-order cyclotron resonance. Through the first-order cyclotron resonance, chorus waves can scatter electrons in both energy and pitch angle spaces, although mainly in pitch angle space [*Kennel and Engelmann*, 1966]. Thus, in principle, the derivative of the electron PSD with respect to pitch angle should subsequently be reduced near the resonant velocity related to the first-order cyclotron resonance. However, lacking reliable information on the original value of this derivative, it is difficult to identify such a signature in the observed electron PSDs. Nevertheless, scattering through the first-order cyclotron resonance, when the corresponding resonant velocity is close to the Landau resonant velocity for some wave events selected, may blur the signatures of Landau resonant interactions examined here and needs further investigations.

Acknowledgments

We are grateful to S. Peter Gary and James P. McFadden for discussion. We acknowledge NASA contract NAS5-02099 and V. Angelopoulos for use of data from the THEMIS Mission. Specifically, we thank C.W. Carlson and J.P. McFadden for use of ESA data and A. Roux and O. LeContel for use of SCM data. The work at Auburn University was supported by NASA grant NNX13AD62G. The analysis at UCLA was supported by the NASA grants NNX11AD75G, NNX11AR64G, and NNX13AI61G.

Larry Kepko thanks the reviewers for their assistance in evaluating this paper.

References

Agapitov, O., A. Artemyev, V. Krasnoselskikh, Y. V. Khotyaintsev, D. Mourenas, H. Breuillard, M. Balikhin, and G. Rolland (2013), Statistics of whistler-mode waves in the outer radiation belt: Cluster STAFF-SA measurements, *J. Geophys. Res. Space Physics*, *118*, 3407–3420, doi:10.1002/jgra.50312.

Agapitov, O. V., A. V. Artemyev, D. Mourenas, V. Krasnoselskikh, J. Bonnell, O. L. Contel, C. M. Cully, and V. Angelopoulos (2014), The quasi-electrostatic mode of chorus waves and electron nonlinear acceleration, *J. Geophys. Res. Space Physics*, *119*, 1606–1626, doi:10.1002/2013JA019223.

Angelopoulos, V. (2008), The THEMIS mission, *Space Sci. Rev.*, *141*(1-4), 5–34, doi:10.1007/s11214-008-9336-1.

Artemyev, A. V., V. V. Krasnoselskikh, O. V. Agapitov, D. Mourenas, and G. Rolland (2012), Non-diffusive resonant acceleration of electrons in the radiation belts, *Phys. Plasmas*, *19*(12), 122901, doi:10.1063/1.4769726.

Artemyev, A. V., A. A. Vasiliev, D. Mourenas, O. V. Agapitov, and V. V. Krasnoselskikh (2013), Nonlinear electron acceleration by oblique whistler waves: Landau resonance vs. cyclotron resonance, *Phys. Plasmas*, *20*(12), 122901, doi:10.1063/1.4836595.

Auster, H. U., et al. (2008), The THEMIS fluxgate magnetometer, *Space Sci. Rev.*, *141*(1-4), 235–264, doi:10.1007/s11214-008-9365-9.

Bonnell, J. W., F. S. Mozer, G. T. Delory, A. J. Hull, R. E. Ergun, C. M. Cully, V. Angelopoulos, and P. R. Harvey (2008), The Electric Field Instrument (EFI) for THEMIS, *Space Sci. Rev.*, *141*(1-4), 303–341, doi:10.1007/s11214-008-9469-2.

Bortnik, J., U. S. Inan, and T. F. Bell (2006), Landau damping and resultant unidirectional propagation of chorus waves, *Geophys. Res. Lett.*, *33*, L03102, doi:10.1029/2005GL024553.

Cattell, C., et al. (2008), Discovery of very large amplitude whistler-mode waves in Earth's radiation belts, *Geophys. Res. Lett.*, *35*, L01105, doi:10.1029/2007GL032009.

Denton, R. E., M. R. Lessard, R. Anderson, E. G. Miftakhova, and W. J. Hughes (2001), Determining the mass density along magnetic field lines from toroidal eigenfrequencies: Polynomial expansion applied to CRRES data, *J. Geophys. Res.*, *106*(A12), 29,915–29,924, doi:10.1029/2001JA000204.

Horne, R. B., and R. M. Thorne (1998), Potential waves for relativistic electron scattering and stochastic acceleration during magnetic storms, *Geophys. Res. Lett.*, *25*(15), 3011–3014, doi:10.1029/98GL01002.

Horne, R. B., R. M. Thorne, S. A. Glauert, J. M. Albert, N. P. Meredith, and R. R. Anderson (2005), Timescale for radiation belt electron acceleration by whistler mode chorus waves, *J. Geophys. Res.*, *110*, A03225, doi:10.1029/2004JA010811.

Kennel, C. F., and F. Engelmann (1966), Velocity space diffusion from weak plasma turbulence in a magnetic field, *Phys. Fluids*, *9*(12), 2377–2388, doi:10.1063/1.1761629.

Kennel, C. F., and H. E. Petschek (1966), Limit on stably trapped particle fluxes, *J. Geophys. Res.*, *71*(1), 1–28, doi:10.1029/JZ071i001p00001.

Koons, H. C., and J. L. Roeder (1990), A survey of equatorial magnetospheric wave activity between 5 and 8 RE, *Planet. Space Sci.*, *38*(10), 1335–1341, doi:10.1016/0032-0633(90)90136-E.

Lauben, D. S., U. S. Inan, T. F. Bell, and D. A. Gurnett (2002), Source characteristics of ELF/VLF chorus, *J. Geophys. Res.*, *107*(A12), 1429, doi:10.1029/2000JA003019.

Le Contel, O., et al. (2008), *First Results of the THEMIS Search Coil Magnetometers*, pp. 222–249, Cambridge Univ. Press, New York.

LeDocq, M. J., D. A. Gurnett, and G. B. Hospodarsky (1998), Chorus source locations from VLF Poynting flux measurements with the Polar spacecraft, *Geophys. Res. Lett.*, *25*(21), 4063–4066, doi:10.1029/1998GL900071.

Li, W., R. M. Thorne, V. Angelopoulos, J. Bortnik, C. M. Cully, B. Ni, O. LeContel, A. Roux, U. Auster, and W. Magnes (2009), Global distribution of whistler-mode chorus waves observed on the THEMIS spacecraft, *Geophys. Res. Lett.*, *36*, L09104, doi:10.1029/2009GL037595.

Li, W., et al. (2010), THEMIS analysis of observed equatorial electron distributions responsible for the chorus excitation, *J. Geophys. Res.*, *115*, A00F11, doi:10.1029/2009JA014845.

Li, W., J. Bortnik, R. M. Thorne, and V. Angelopoulos (2011), Global distribution of wave amplitudes and wave normal angles of chorus waves using THEMIS wave observations, *J. Geophys. Res.*, *116*, A12205, doi:10.1029/2011JA017035.

Li, W., R. M. Thorne, J. Bortnik, X. Tao, and V. Angelopoulos (2012), Characteristics of hiss-like and discrete whistler-mode emissions, *Geophys. Res. Lett.*, *39*, L18106, doi:10.1029/2012GL053206.

Li, W., J. Bortnik, R. M. Thorne, C. M. Cully, L. Chen, V. Angelopoulos, Y. Nishimura, J. B. Tao, J. W. Bonnell, and O. LeContel (2013), Characteristics of the Poynting flux and wave normal vectors of whistler-mode waves observed on THEMIS, *J. Geophys. Res. Space Physics*, *118*, 1461–1471, doi:10.1002/jgra.50176.

Liu, K., S. P. Gary, and D. Winske (2011), Excitation of banded whistler waves in the magnetosphere, *Geophys. Res. Lett.*, *38*, L14108, doi:10.1029/2011GL048375.

McFadden, J. P., C. W. Carlson, D. Larson, V. Angelopoulos, M. Ludlam, R. Abiad, B. Elliott, P. Turin, and M. Marckwordt (2008), The THEMIS ESA plasma instrument and in-flight calibration, *Space Sci. Rev.*, *141*(1-4), 277–302, doi:10.1007/s11214-008-9440-2.

Meredith, N. P., R. B. Horne, A. Sicard-Piet, D. Boscher, K. H. Yearby, W. Li, and R. M. Thorne (2012), Global model of lower band and upper band chorus from multiple satellite observations, *J. Geophys. Res.*, *117*, A10225, doi:10.1029/2012JA017978.

Omura, Y., Y. Katoh, and D. Summers (2008), Theory and simulation of the generation of whistler-mode chorus, *J. Geophys. Res.*, *113*, A04223, doi:10.1029/2007JA012622.

Parrot, M., O. Santolík, N. Cornilleau-Wehrlin, M. Maksimovic, and C. C. Harvey (2003), Source location of chorus emissions observed by cluster, *Ann. Geophys.*, *21*(2), 473–480, doi:10.5194/angeo-21-473-2003.

Qin, Z., R. E. Denton, N. A. Tsyganenko, and S. Wolf (2007), Solar wind parameters for magnetospheric magnetic field modeling, *Space Weather*, *5*, S11003, doi:10.1029/2006SW000296.

Roux, A., O. L. Contel, C. Coillot, A. Bouabdellah, B. de la Porte, D. Alison, S. Ruocco, and M. C. Vassal (2008), The search coil magnetometer for THEMIS, *Space Sci. Rev.*, *141*, 265–275, doi:10.1007/s11214-008-9455-8.

Santolík, O., and D. A. Gurnett (2003), Transverse dimensions of chorus in the source region, *Geophys. Res. Lett.*, *30*(2), 1031, doi:10.1029/2002GL016178.

Santolík, O., F. Lefeuvre, M. Parrot, and J. L. Rauch (2001), Complete wave-vector directions of electromagnetic emissions: Application to INTERBALL-2 measurements in the nightside auroral zone, *J. Geophys. Res.*, *106*(A7), 13,191–13,201, doi:10.1029/2000JA000275.

Santolík, O., D. A. Gurnett, J. S. Pickett, M. Parrot, and N. Cornilleau-Wehrlin (2003), Spatio-temporal structure of storm-time chorus, *J. Geophys. Res.*, *108*(A7), 1278, doi:10.1029/2002JA009791.

Santolík, O., D. Gurnett, J. Pickett, M. Parrot, and N. Cornilleau-Wehrlin (2005), Central position of the source region of storm-time chorus, *Planet. Space Sci.*, *53*(1-3), 299–305, doi:10.1016/j.pss.2004.09.056.

Santolík, O., D. A. Gurnett, J. S. Pickett, J. Chum, and N. Cornilleau-Wehrlin (2009), Oblique propagation of whistler mode waves in the chorus source region, *J. Geophys. Res.*, *114*, A00F03, doi:10.1029/2009JA014586.

Stix, T. H. (1962), *The Theory of Plasma Waves*, McGraw-Hill, New York.

Swanson, D. G. (2003), *Plasma Waves*, pp. 333–335, 2nd ed., Inst. of Phys., Philadelphia, Pa.

Tsurutani, B. T., and E. J. Smith (1974), Postmidnight chorus: A substorm phenomenon, *J. Geophys. Res.*, *79*(1), 118–127, doi:10.1029/JA079i001p00118.

Tsurutani, B. T., and E. J. Smith (1977), Two types of magnetospheric ELF chorus and their substorm dependences, *J. Geophys. Res.*, *82*(32), 5112–5128, doi:10.1029/JA082i032p05112.

Tsyganenko, N. A., and M. I. Sitnov (2005), Modeling the dynamics of the inner magnetosphere during strong geomagnetic storms, *J. Geophys. Res.*, *110*, A03208, doi:10.1029/2004JA010798.

Verkhoglyadova, O. P., B. T. Tsurutani, and G. S. Lakhina (2010), Properties of obliquely propagating chorus, *J. Geophys. Res.*, *115*, A00F19, doi:10.1029/2009JA014809.